Microplasma source for optogalvanic spectroscopy of nanogram samples

M. Berglund, G. Thornell, and A. Persson

Citation: J. Appl. Phys. **114**, 033302 (2013); doi: 10.1063/1.4813414
View online: http://dx.doi.org/10.1063/1.4813414
View Table of Contents: http://jap.aip.org/resource/1/JAPIAU/v114/i3
Published by the AIP Publishing LLC.

Microplasma source for optogalvanic spectroscopy of nanogram samples

M. Berglund,[1] G. Thornell,[1] and A. Persson[1,2]
[1]*Ångström Space Technology Centre, Department of Engineering Sciences, Uppsala University, Box 534, SE-75121 Uppsala, Sweden*
[2]*Department of Physics and Astronomy, Ion Physics, Uppsala University, Box 516, SE-75120 Uppsala, Sweden*

(Received 14 May 2013; accepted 21 June 2013; published online 15 July 2013)

The demand for analysis of smaller samples in isotopic ratio measurements of rare isotopes is continuously rising with the development of new applications, particularly in biomedicine. Interesting in this aspect are methods based on optogalvanic spectroscopy, which have been reported to facilitate both ^{13}C-to-^{12}C and ^{14}C-to-^{12}C ratio measurements with high sensitivity. These methods also facilitate analysis of very small samples, down to the microgram range, which makes them very competitive to other technologies, e.g., accelerator mass spectroscopy. However, there exists a demand for moving beyond the microgram range, especially from regenerative medicine, where samples consist of, e.g., DNA, and, hence, the total sample amount is extremely small. Making optogalvanic spectroscopy of carbon isotopes applicable to such small samples, requires miniaturization of the key component of the system, namely the plasma source, in which the sample is ionized before analysis. In this paper, a novel design of such a microplasma source based on a stripline split-ring resonator is presented and evaluated in a basic optogalvanic spectrometer. The investigations focus on the capability of the plasma source to measure the optogalvanic signal in general, and the effect of different system and device specific parameters on the amplitude and stability of the optogalvanic signal in particular. Different sources of noise and instabilities are identified, and methods of mitigating these issues are discussed. Finally, the ability of the cell to handle analysis of samples down to the nanogram range is investigated, pinpointing the great prospects of stripline split-ring resonators in optogalvanic spectroscopy. © *2013 AIP Publishing LLC*. [http://dx.doi.org/10.1063/1.4813414]

I. INTRODUCTION

Highly sensitive measurements of isotopic ratios have a wide range of applications, from medicine to archaeology. Most renowned are maybe measurements of long-lived radioisotopes such as ^{14}C, ^{10}Be, and ^{129}I that can be used for, e.g., dating organic deposits in archaeology,[1,2] and rocks and sediments in geology.[3,4] However, ^{14}C measurements have also proven useful for isotopic labelling of drugs in clinical trials by microdosing[5] and for studying cell regeneration in the human body.[6,7] Such new applications, along with rising demands from the traditional clients, have created an increasing call for more sensitive and less expensive measurement methods, and, even more important, methods that allow for smaller sample sizes.

Traditionally, radioisotopes have been measured by scintillation techniques, such as liquid or gas scintillation counting (LSC or GSC).[8,9] These techniques count the number of radioactive decays in the sample over a given period of time, yielding the relative amount of the studied radioisotope from its half-life. However, scintillation techniques require fairly large samples in order to get acceptable statistics in the measurement, since the isotopes of interest to dating in archaeology and geology, by definition, have a relatively long half-life (5760 years for ^{14}C and 1.5 million years for ^{9}Be). For example, an LSC typically requires more than one gram of graphite to register 10 atomic disintegrations per minute.[6]

In many applications, samples of this size are difficult to acquire. In the case of archaeology, questions regarding context, preservation, and contamination often set limitations to which samples that can be applicable to radiocarbon dating, meaning that it is not always the largest pieces that are the most interesting. Moreover, the initial sample preservation and preparation process has a limited yield in terms of carbon content. In the case of medicine, samples are sometimes in the form of biopsies, where the limit to the sample size is obvious, especially if the sample is, e.g., brain tissue. For these reasons, other measurement techniques allowing for smaller sample sizes, such as accelerator mass spectroscopy (AMS), have conquered a large part of the market, even though the cost per sample analysis is higher. In contrast to scintillation-based techniques, AMS takes all atoms of a certain isotope into account, and not only those who disintegrate. This fundamental difference makes AMS both more sensitive and less sample consuming than, e.g., LSC. Current AMS technology allows for sub-attomole sensitivity with samples in the 0.01–1 mg range.[6,10,11]

In the case of AMS, the limiting factor with regard to sample size is the sample preparation process. This process includes steps of oxidation, graphitization, and ionization, each having a different yield in terms of carbon content, where the minimum sample size is set by the restriction of having a sufficient detection rate in the final accelerator stage.[12] The risks of contamination in the preparation process also increase as the sample size is reduced. Attempts of

miniaturizing parts of the sample preparation system have proven successful in reducing the minimum sample size down towards the microgram region.[6] However, reducing the sample size even further may prove technologically difficult, wherefore new measurement techniques with similar sensitivity, but based on different physical principles, have rendered an increasing attention.[13,14]

One such technique is intracavity optogalvanic spectroscopy (ICOGS) which has been reported to be as sensitive as AMS.[14] ICOGS is based on the optogalvanic effect (OGE), which refers to the response of a discharge or plasma to an optical perturbation. When the plasma is illuminated with radiation of the same wavelength as, e.g., one of the ro-vibrational transitions of the molecules in the plasma, the molecules are excited into that particular ro-vibrational state—something that affects the mobility of the electrons in the plasma, and, hence, changes the plasma impedance. The impedance can be measured directly by inserting Langmuir probes into the plasma, or indirectly by measuring the input power to the plasma source.[14,15] The change in impedance is directly proportional to the number of excited molecules in the plasma, and, with a well defined radiation source, e.g., a laser, the change in impedance can even be related to the number of molecules of that particular species and, hence, be used for spectrometric applications. The technique of measuring the abundance of different molecules using the OGE is called optogalvanic spectroscopy (OGS).[16]

By using an isotope-specific CO_2 laser as the source of the radiation, i.e., a laser with a wavelength identical to one of the isotope-specific transitions in the mid-IR spectra of CO_2, it has been shown that OGS is applicable to measurements of the isotopic composition of carbon samples. Murnick *et al.* have shown that OGS is capable of measuring the ratio of ^{13}C-to-^{12}C[17] with applications in, e.g., ulcer diagnostics, and possibly even the ^{14}C-to-^{12}C ratio using the formerly mentioned ICOGS technique.[14,16] In both embodiments, the analyzed carbon is in the form of CO_2. In ordinary OGS, the ionized sample is located in the laser beam path, whereas in ICOGS, the sample is inserted into the laser cavity itself. The intracavity approach has been reported to increase the sensitivity by almost seven orders of magnitude compared with ordinary "extracavity" OGS.[14]

Although the narrow line-width ro-vibrational absorption lines of CO_2 in the mid-IR spectrum facilitate analysis of the isotopic composition of both carbon and oxygen, issues relating to background from spectral broadening of nearby absorption lines as well as from other molecules have to be properly addressed in a high-precision measurement. Measurements of the ^{13}C-to-^{12}C ratio are relatively straightforward, since the natural abundance of ^{13}C is about 1%.[18] The ^{14}C-to-^{12}C ratio, on the other hand, puts tremendously higher requirements on the sensitivity, since the natural abundance of ^{14}C is only in the order of 10^{-12}. The most prominent source of background when applying OGS to ^{14}C measurements is collision broadening of the absorption lines of $^{12}CO_2$ and $^{13}CO_2$.[14] Somewhat counterintuitive, a recent study has shown that it is not the $^{12}CO_2$ and $^{13}CO_2$ lines closest to the investigated $^{14}CO_2$ line that contribute the most to the background, but the lines with the highest Boltzmann population, even though these can be situated more than a micrometer away.[15] Moreover, it has recently been shown that ICOGS suffers from considerable problems with the stability and reproducibility of the optogalvanic signal, raising questions on the actual applicability of the method to radiocarbon measurements.[19] However, concurrent ICOGS employs almost 30 years old technology for measuring the OGE.[20] Hence, a new, more stable and reliable, measurement technique will benefit ICOGS.

OGS can handle samples in the sub-microgram range,[14,16] partly because of the simplified sample preparation, where, in contrast to AMS, only oxidation is required. In the case of OGS, the limiting factor for the sample size is instead the amount of carbon that is required to fill the plasma chamber, in which the sample is ionized, to an adequate pressure. This chamber is typically a vacuum sealed cavity equipped with a plasma source for ionizing the sample, and Brewster angle windows for reflection-free transmission of the laser beam through the cell. The diameter of the laser beam, the volume of the plasma, and pressure in the chamber have been reported to affect the sensitivity.[16] In order to minimize the sample size, it would be convenient to minimize the plasma volume so that less CO_2 is required to keep the cavity at a certain pressure. This would, in turn, require miniaturization of the plasma source.

In the study presented here, the applicability of such a microplasma source (MPS), based on a split-ring resonator (SRR),[21] to OGS has been investigated experimentally. The MPS was integrated in an extracavity OGS system, and the dependency of the optogalvanic signal on the frequency and power of the plasma, as well as on the pressure and flow of CO_2, and the modulation frequency of the laser was investigated. The stability of the signal with respect to these parameters as well as the limitations of the miniaturization were also studied.

II. THEORY

There are different explanations to the OGE depending on which particle species that populate the plasma. In the case of an atomic plasma, the incident radiation affects the ionization balance, by exciting the atoms to energy levels with either higher or lower ionization probability, and thus changes the plasma impedance.[22] This effect is less pronounced in the case of a molecular plasma, as in the case of this study, and the main process behind the OGE here is instead that the radiation establishes alternative decay paths from the radiation-excitation levels, via absorption or stimulated emission.[23] This causes a change in the plasma equilibrium temperature from the change in the gas number density, which in turn affects the collision frequency and thereby the mobility of electrons in the plasma. Depending on whether the change in gas number density has a heating or cooling effect, the change in mobility either increases or reduces the plasma impedance.

Under the assumption that the collision frequency of the plasma is much higher than the frequency at which the plasma source is operated and that the density of neutral molecules is much higher than the density of electrons, i.e.,

that the distribution function of the electrons is strongly dependent on collisions with molecules, the impedance change, or the optogalvanic signal, S, in a plasma, irradiated with a laser beam of intensity I at frequency f, can be approximated by the integral

$$S = \iiint_V n(r,\theta,z)I(r,\theta,z,f)\sigma(f)K dx dy dz, \quad (1)$$

where n is the number density of the investigated species, $\sigma(f)$ is the stimulated emission or absorption cross section, V is the volume of the irradiated part of the plasma, and K is the so called optogalvanic proportionality constant which accounts for irregularities in the plasma conditions from, e.g., pressure, flow, and temperature.[16]

Assuming the laser beam to be cylindrical with a narrower distribution than the plasma itself, Fig. 2, and K to be independent of n, Eq. (1) can be approximated by[16]

$$S = nI\sigma K\pi LR^2, \quad (2)$$

given that the laser beam cross-section is completely within the plasma, exposing a cylindrical volume of length L and radius R.

III. MATERIALS AND METHODS

A. Manufacturing

The MPSs investigated here were stripline SRRs, Fig. 1, closely resembling those described in Ref. 24. The stripline concept was chosen to avoid electromagnetic interference in the measurements, simultaneously as the transverse hole through the gap constituted a miniature plasma chamber allowing for extremely small samples to be analyzed. Separating the SRRs of this study from those described in Ref. 24 was the addition of two plasma probes with associated pads, Figs. 1 and 2, which were extended into the gap, orthogonally to the SRR electrodes and the laser beam path.

The SRR MPSs were manufactured on a printed circuit board (4003 C, Rogers Corp., USA) with a thickness of 1.524 mm, a dielectric constant, ε_R, of 3.38, and a loss tangent, tanδ, of 0.0022. The MPSs were manufactured using a milling machine (S100, LPKF, USA). The resonator ring had an inner radius of 4.23 mm and an outer radius of 6.03 mm. The feed point was positioned at an angle of 167.7° from the gap, Fig. 1, which was 2 mm wide. The feed strip had the same width as the ring, i.e., 2.20 mm, making the design of the resonator part of MPSs identical to the 50 Ω stripline SRRs in Ref. 21.

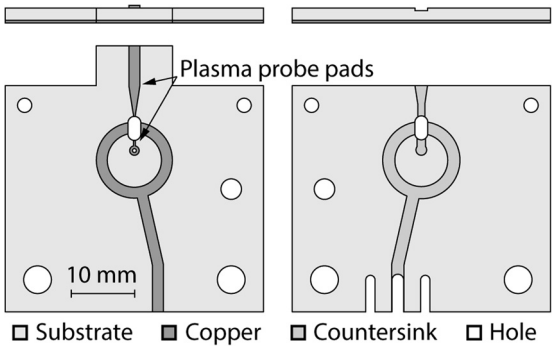

FIG. 1. Schematic drawing of the two halves of the SRR with the added plasma probe pads.

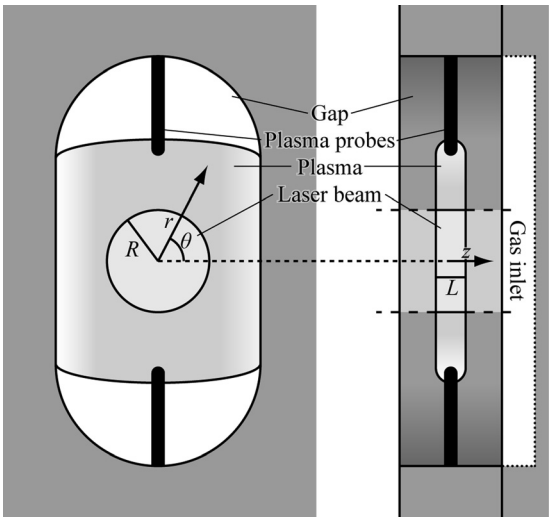

FIG. 2. Close-up of the plasma and the laser beam in the gap of the MPS, seen from the view corresponding to that of Fig. 1 (left) and in cross section from the side (right). The plasma bridges the SRR electrodes on the elongated sides of the gap, while the laser beam is aligned in the centre of the gap between the plasma probes. The sample gas is introduced perpendicularly to the gap, 1.5 mm from the electrodes.

MPSs were equipped with plasma probes, consisting of 25 μm thick gold wires, which were bonded to the probe pads, Fig. 1, using a wedge bonder (4526, Kulicke & Soffa, Singapore). Each probe was extended approximately 1 mm into the gap, Fig. 2. One probe was connected to one of the SRR ground planes, whereas the other one was connected to an SMA coaxial cable socket. This contact was used to measure the optogalvanic signal.

To make sure that an introduced CO_2 sample entered the gap of the MPSs, the plasma sources were equipped with a fluidic system, placing the gas inlet only 1.5 mm from the SRR electrodes, Fig. 2 (right). Like with the plasma sources, the fluidic system was manufactured from a PCB by milling, and stacked on top of the MPSs by gluing. One such fluidic system was connected to each side of the MPS to accommodate easy mounting and connection, Fig. 3.

B. Setup

The electronics used for controlling and analyzing the plasma consisted of an radio frequency (RF) wave generator with variable power attenuation, A_p, and frequency, f_p, and an RF characterization unit measuring the power and phase of the RF wave transmitted to and reflected from the plasma source. Both units were controlled by a computer. The electronics is described schematically in Fig. 4 and more thoroughly in Ref. 24.

The MPSs were mounted inside a vacuum chamber with electrical connections for power input and signal output. All OGE measurements were made inside the chamber by introducing a variable amount of CO_2 (Air Liquid, France), through the fluidic system, which was connected to the gas

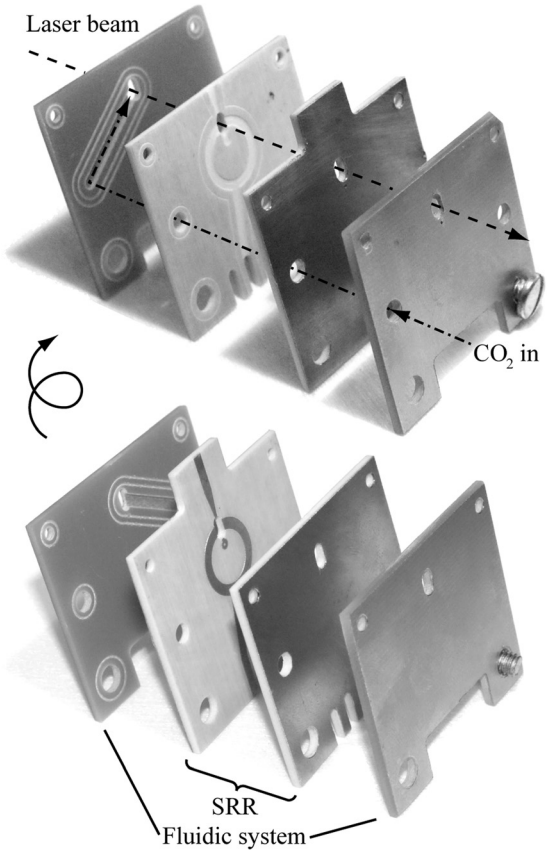

FIG. 3. Exploded view of an MPS with a 2 mm gap and a double sided fluidic system.

inlet of the vacuum chamber via a plastic tube. The chamber was equipped with an antireflection coated ZnSe window (WG71050-F, Thorlabs Inc., USA) for transmission of the CO_2 laser beam, a pressure gauge (275 Mini-Convector, Brooks Automation Inc., USA) for internal pressure measurements, and a vent with a mass flow controller (F-200, Bronkhorst Hi-Tech, The Netherlands), which had a dynamic range of 0-100 sccm, for controlling and monitoring the inflow of CO_2, m, Fig. 5. The pressure gauge and the flow controller were connected to a computer and controlled by custom made software (MATLAB R2012a, Mathworks, USA). The base pressure of the chamber was around 230 Pa.

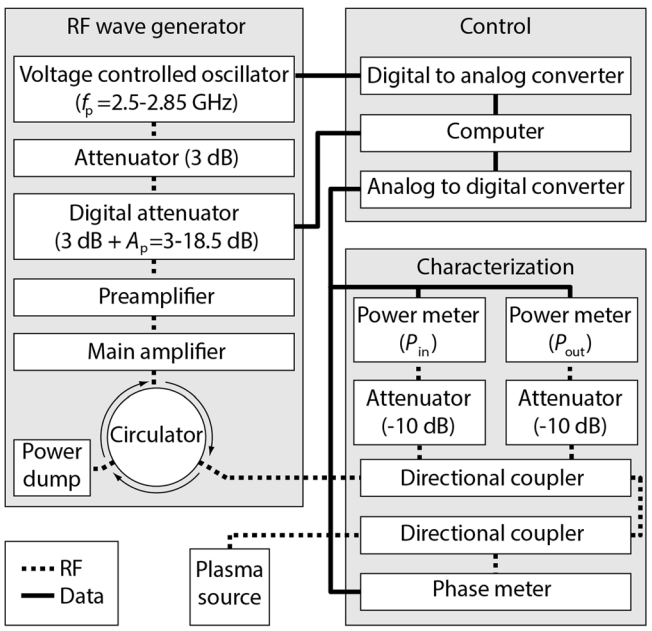

FIG. 4. Schematic view of the RF electronics.

The MPS, inside the vacuum chamber, was incorporated in an extracavity OGS consisting of an CO_2 laser (J48-1 S, Synrad Inc., USA) with a maximum output power, P_L, of 30 W, an optical chopper (Model 9475, Brookdeal Inc., USA) with a variable chopping frequency, f_C, in the range of 10 Hz and 1 kHz, and an antireflection-coated focussing ZnSe lens (LA7028-F, Thorlabs Inc., USA) with a focal length of 150 mm, Fig. 5. The lens was aligned so that it focused the laser beam approximately at the centre of the gap of the MPS.

The alignment was performed by first aligning the beam of an HeNe laser, with a visible wavelength, coaxially with the CO_2 laser beam, by letting both beams run through two parallel irises. The HeNe beam was then used to align both beams to the gap of the MPS. The final alignment was performed by studying the interference of the HeNe beam on the plasma probe bond wires, by which the beams could be aligned in the centre of the gap, between the ends of the probes, Fig. 2.

C. Measurements

The optogalvanic signal was measured by an oscilloscope (DSO7104A, Agilent Tech., USA) connected to one of the plasma probes of the MPSs via an SMA coaxial cable. The oscilloscope was also connected to the reference channel of the chopper to accommodate triggering on the correct frequency. The signal was AC coupled to remove the DC component of the voltage between the plasma probes, i.e., only the dynamic part of the optogalvanic signal was taken into account. The signal was measured in the time domain with 8-bit resolution at adjustable amplification and sampling frequency, accommodating high resolution characterization of the plasma impedance, and thereby of the OGE.

D. Post processing

The sampled time series were sent to the computer for post processing. The time samples were transformed to the frequency domain using the fast Fourier transform (FFT) algorithm after being zero-padded to increase the frequency resolution. The optogalvanic signal, S, was defined as the integral of the spectrum over a ± 10 Hz frequency range centred at f_C, to accommodate some instability in the chopper frequency. The signal-to-noise ratio (SNR) of S was improved by averaging.

E. Experiments

The setup had a number of variable parameters that affected the optogalvanic signal, in particular m, A_P, f_P, and f_C. After some initial proof-of-concept tests, a set of four experiments, each varying one parameter at a time, was designed, in order to investigate these parameters' influence

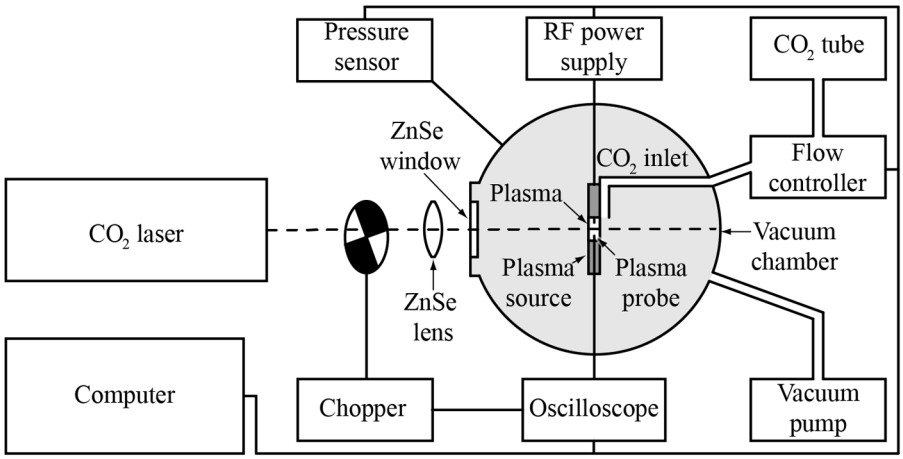

FIG. 5. Schematic view of the OGS.

on the optogalvanic signal. In a fifth experiment, all parameters were kept constant while the laser beam was moved across the gap. The settings of each parameter during the five experiments, here referred to as experiment I–V, are presented in Table I. The laser power was kept constant at 10 W throughout all experiments.

IV. RESULTS

Initially, the work was directed towards verifying the function of the system as a whole, and that the SRRs could actually be used for measuring the optogalvanic signal. In order to do so, the vacuum chamber was flushed with CO_2 up to a pressure of more than 3000 Pa, where the MPSs still could be ignited, and the output signal was measured as the laser was turned on. A clear optogalvanic signal could be detected, where both the modulation of the chopper ($f_C = 250$ Hz) and of the pulse width in the laser ($f_{PWM} = 5$ kHz) clearly could be seen, Fig. 6. Changing the settings to those of experiment V, a typical SNR of the system was estimated to around 27 dB, by dividing the amplitude of the spectrum at f_C, i.e. the maximum of the OGE peak, by the median of the spectrum, Fig. 6 (inset).

In experiment I, the dependency of S on m was investigated. To further verify the function of the MPSs in measuring the optogalvanic signal, the experiment was repeated but the gas tube CO_2 was replaced with air, having a CO_2 content of 0.035%, Fig. 7. As expected, S was more or less independent of the inflow of air but showed a clear dependence on the inflow of CO_2.

In experiment II, the dependency of S on A_P was investigated. Reducing the attenuation of the power from the RF amplifier corresponded to increasing the power into the plasma source, P_{in}, affecting the electrical field in the gap of

TABLE I. Settings of the CO_2 flow, m, plasma attenuation, A_P, plasma frequency, f_P, and chopper frequency, f_C, in the five experiments.

Experiment	m [sccm]	A_P [dB]	f_P [GHz]	f_C [Hz]
I	0–85 (CO_2 or Air)	10	2.80	270
II	40 (CO_2)	0–21.5	2.80	170
III	40 (CO_2)	10	2.73–2.85	170
IV	40 (CO_2 or Air)	10	2.80	10–520
V	40 (CO_2 or Air)	10	2.80	170

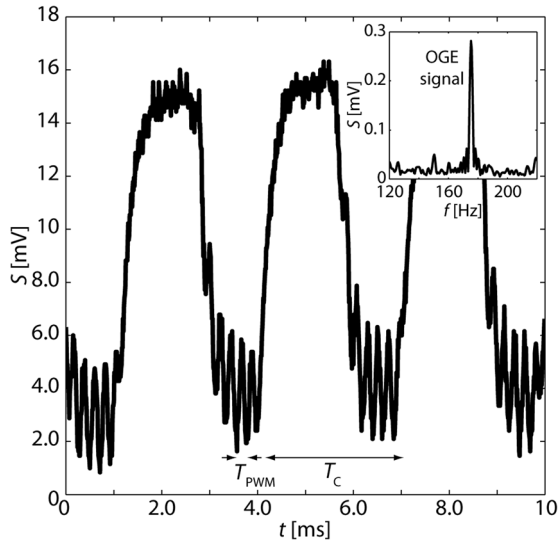

FIG. 6. Optogalvanic signal, S, with a CO_2 pressure of 3000 Pa in the vacuum chamber. T_C and T_{PWM} correspond to the period time of the modulation of the chopper and of the pulse width modulation of the laser, respectively. The inset shows a typical OGE spectrum from experiment V.

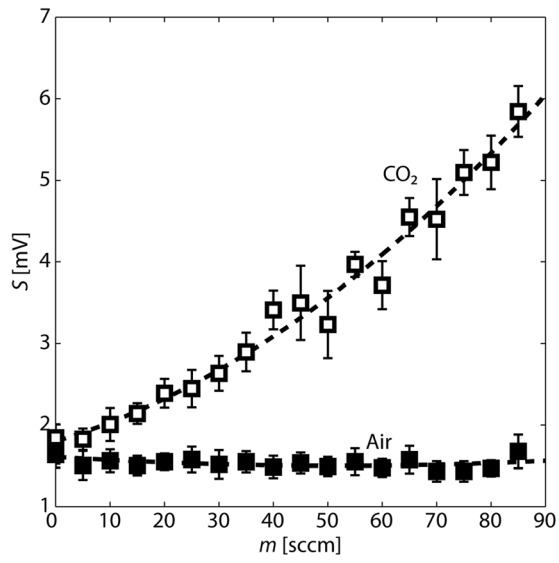

FIG. 7. Optogalvanic signal, S, as a function of the inflow, m, of CO_2 (white squares) and air (black squares), respectively.

the MPSs and thereby the intensity and impedance of the plasma. To study how different attenuation affected the plasma, the voltage over the plasma probes, U, was recorded in addition to the dynamic voltage, containing the optogalvanic signal. The amplitude and stability of S at different P_{in} are shown in Fig. 8 (top). Here, the amplitude and stability were described by the mean and the standard deviation, σ, of 20 consecutive measurements. As a reference, the change in U, $\partial U/\partial P_{in}$, as a function of P_{in} is shown in Fig. 8 (bottom), given the assumption that the amplitude of S is related to how much a small change in P_{in} could change U, i.e., how sensitive the plasma was to small perturbations.

Similarly, experiment III studied the dependency of S on f_P. As for changing the attenuation, shifting the frequency of the RF fed into the SRR away from resonance too changed P_{in}, and ultimately the impedance of the plasma. However, the resonance behaviour of an ignited SRR is not the same as that of an un-ignited one, since the plasma changes the dielectric properties in the gap, wherefore the optimum f_P from an OGS point of view was not obvious. To study how different f_P affected the plasma, U was again recorded in addition to S. The amplitude and stability of S at different f_P are shown in Fig. 9 (top). As before, the amplitude and stability were described by the mean and the standard deviation of 20 consecutive measurements. The derivative $\partial U/\partial f_P$ as a function of f_P is shown as a reference in Fig. 9 (bottom), given the same assumption as in experiment II. The plasma went out just below $f_P = 2.73$ GHz, whereas the electronics could only deliver RF up to 2.85 GHz, at which the plasma still was ignited.

Experiment IV focused on the modulation frequency of the chopper, having implications on both the operation of the MPS, and on the implementation of the data processing.

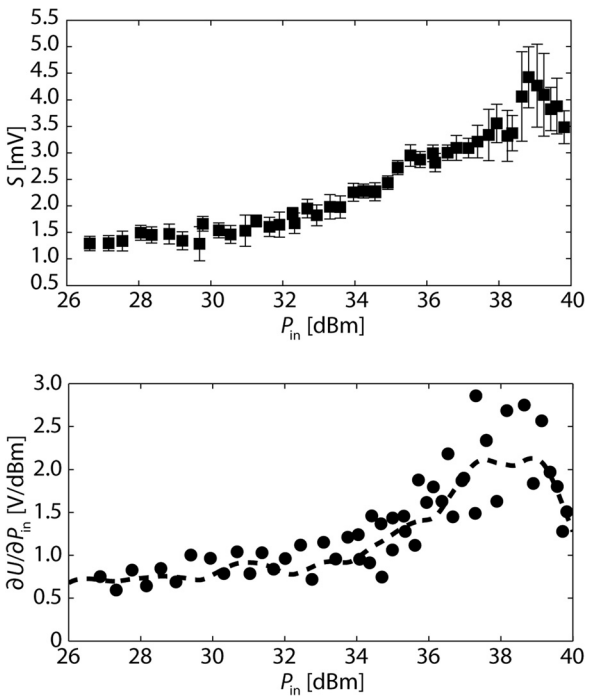

FIG. 8. Dependency of S on P_{in} (top), and the dependency of $\partial U/\partial P_{in}$ on P_{in} (bottom).

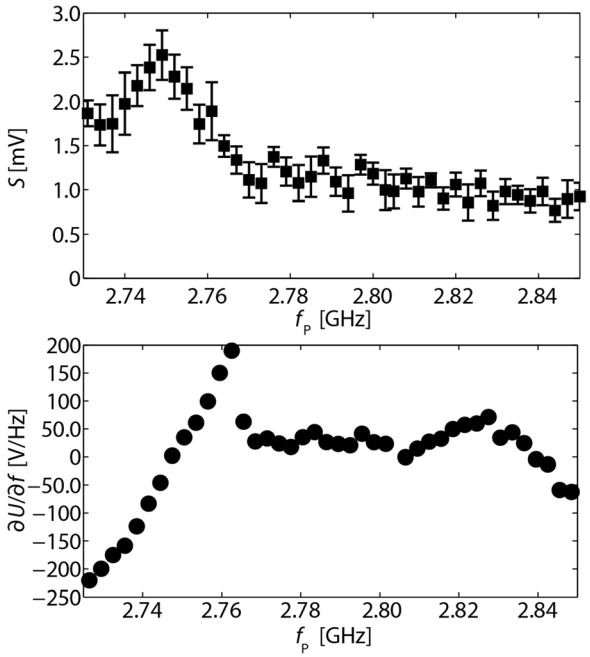

FIG. 9. Dependency of S (top) and $\partial U/\partial f_P$ (bottom) on f_P.

Like in experiment I, measurements with inflow of both CO_2 and air were performed to investigate if the period time of the IR irradiation from the laser would cause any thermal background to S. Moreover, the post processing of the data in experiment IV only took the amplitude of the first harmonic of S into account, i.e. no integration over the peak was performed. This was done to allow for comparison of measurements made at different sampling rates, although it made it difficult to quantitatively compare the results from experiment IV with those of the rest of the experiments. However, qualitative comparisons were still possible. Only regarding the first harmonic of S made the waveform of the optogalvanic signal important. The waveform was, in turn, dependent on f_C. The results of experiment IV can be found in Fig. 10.

The final experiment, V, focused on studying the effect of the position of the laser beam in the gap of the MPSs. The beam, which was initially centred in the gap, was stepwise moved towards the side of the gap, perpendicularly to the plasma probes, of an MPS, Fig. 11. Close to the wall, S increased abruptly. However, replacing the inflow of CO_2 with air showed that this increase was not dependent on the amount of CO_2 in the chamber, and thus not on the OGE, in contrast to the signal in the centre of the gap, which showed a similar characteristic as in experiment I. Additional experiments with an MPSs with a 1 mm gap were performed, but it was found that proper alignment of the laser beam was difficult over a longer time span with such devices, due to mechanical drift in the mounting of the MPS.

V. DISCUSSION

The experiments showed that the SRR MPSs could in fact be used for OGS. However, the stability of the signal and the SNR were relatively low. Averaging generally improves the SNR by the square root of the number of

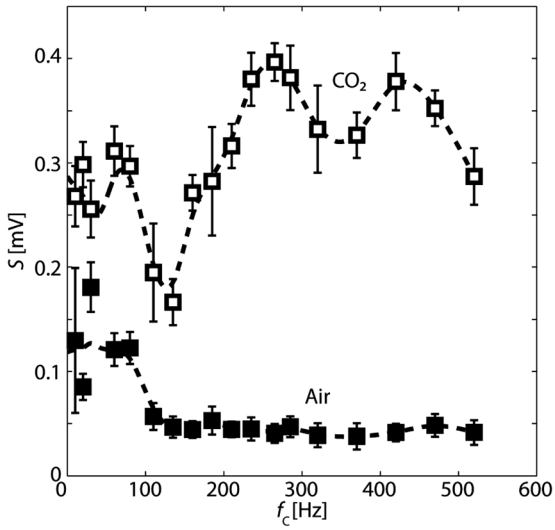

FIG. 10. Optogalvanic signal, S, as a function of the chopper frequency, f_C, at an inflow of 40 sccm CO_2 (white squares) and 40 sccm air (black squares), respectively.

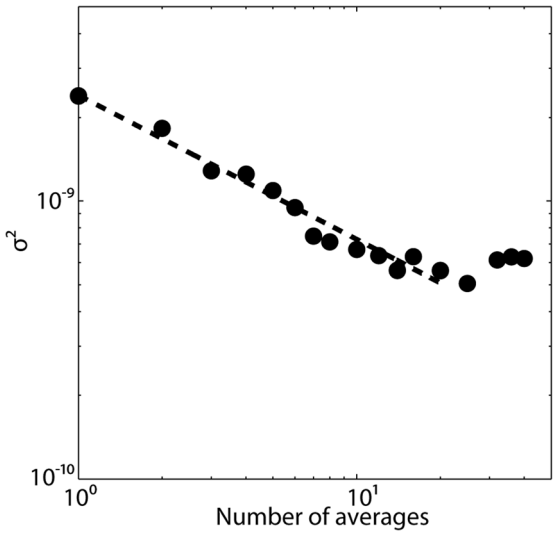

FIG. 12. Allen variance analysis yielding the optimum number of averages to be ~20. The dashed line shows the square root dependence of the variance to the number of averages over limited measurement times.

averages, but only up to the point where long-time drift, e.g., temperature or mechanical, becomes a limiting factor, cancelling the positive effect of the averaging on the precision of the measurement.

To study the stability of our system, the variance of up to 40 averages from experiment V, with 40 sccm CO_2 introduced into the chamber, was analysed, Fig. 12. Each measurement point took approximately 1 s to record, wherefore the number of averages can be translated into the total measurement time in seconds. Over shorter intervals, the variance showed the expected square root dependence, but for measurement times longer than 20 s, i.e., more than 20 averages, the SNR improvement levelled out. In our system, intensity drift in the laser, thermal drift in the electronics powering the MPS, and flow-rate drift in the fluidic system were assumed to be the major limitations to the maximum number of averages. Employing active temperature control

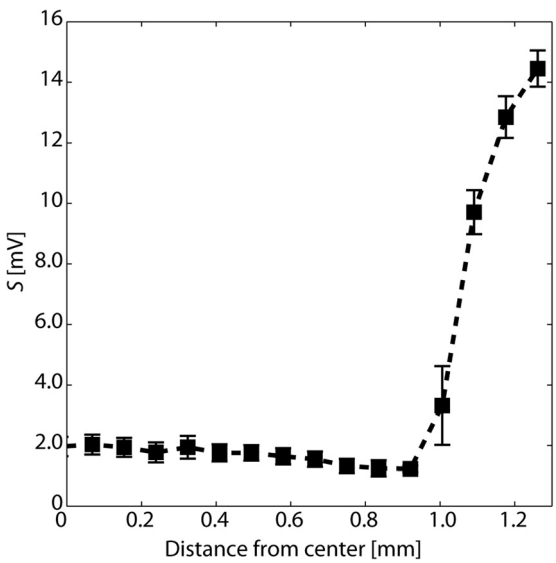

FIG. 11. Optogalvanic signal, S, as the laser beam is moved perpendicularly to the plasma probes from the centre of the gap towards the side.

of the laser, electrical shielding, and improved passive cooling of the electronics, and, ultimately, more precise hardware, are expected to improve the long time stability of the system and allow for extended averaging, and hence improved SNR.

Just as important to optimize were the operational parameters of the MPS and the OGS. Experiments I-IV showed that m, A_P, f_P, and f_C all influenced both the amplitude and the stability of S. In order to study the effect of these parameters on the precision of the measurements, the signal-to-standard deviation ratio, S/σ, was analyzed, Fig. 13.

In experiment I, the amplitude of S increased with an increasing flow of CO_2 into the chamber, Fig. 7. This was well in line with Eqs. (1) and (2) predicting an increased signal when the number of CO_2 molecules in the irradiated part of the plasma increased. Moreover, higher flow caused the pressure in the chamber to rise, Fig. 14 (inset), which influenced the dielectric properties in the gap of the MPS, thereby shifting both the intensity and the static impedance of the plasma, influencing the parameters K and L in Eq. (2). This latter effect was thought to be the main cause for the deteriorating plasma stability as the flow increased, Fig. 13(a). By visual inspection, it could be seen that the plasma started to flicker at higher flow rates. This was attributed to instabilities in the flow control, and to slipping phenomena[25] and/or turbulence at the gas inlet. Flicker noise—also known as $1/f$ noise due to its inverse frequency dependence—is a very common phenomenon, occurring in almost every physical process (from spin-ordering in magnetic materials[26] to highway traffic patterns[27]). The power spectral density of flicker noise, $S_{1/f}$, in electromagnetic systems can be empirically described by the Hooge equation[28]

$$S_{1/f} = V^2 \alpha_H (N_C f)^{-1}, \tag{3}$$

where V is the voltage, f is the frequency, N_C is the number of charge carriers in the system, and α_H is the phenomenological Hooge parameter.

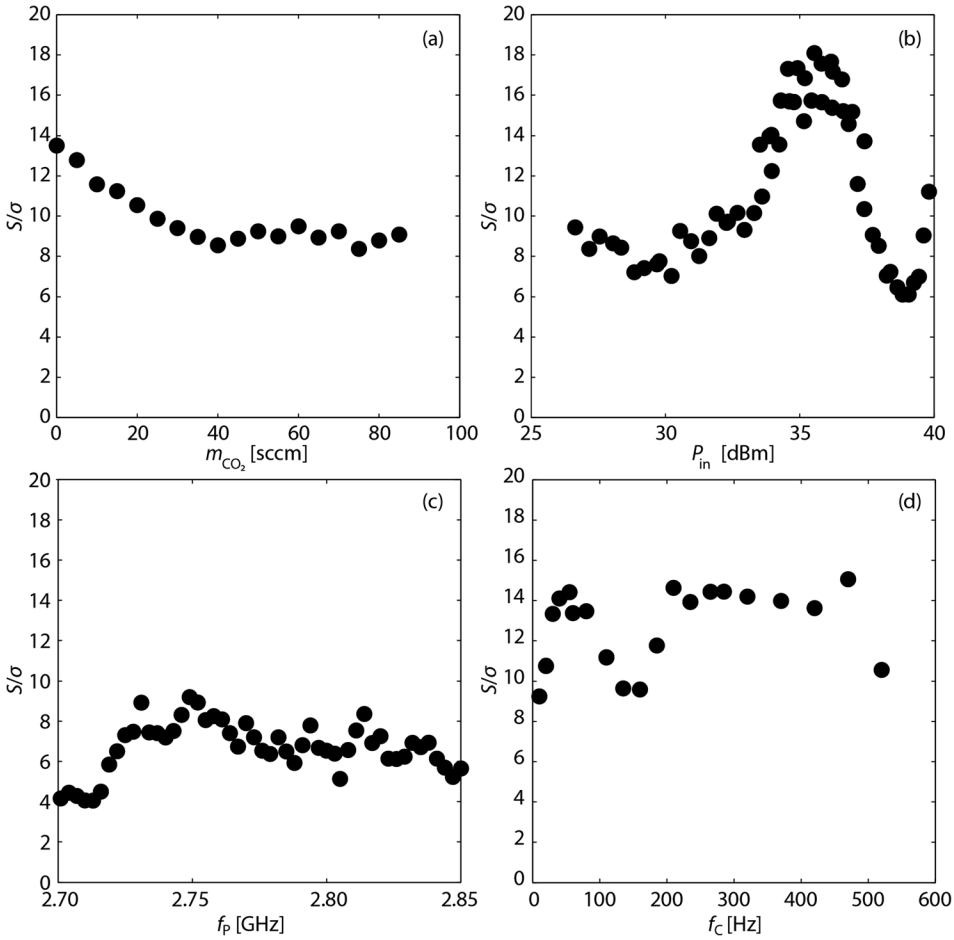

FIG. 13. Signal-to-standard deviation ratio, S/σ, in experiment I (a), II (b), II (c), and IV (d), respectively.

To investigate if the instabilities observed in the flow measurements could be translated as $1/f$ noise, the noise floor of the spectrum at different m was curve fitted to a function on the form $af^{b}+c$, where the constant $a=V(\alpha_H/N_C)^{0.5}$ contained the information on the $1/f$ noise density, Fig. 14. To account for the variations in N_C and V at different flows, a was scaled by the measured pressure and plasma potential, assuming ideal gas conditions, Fig. 14 (inset). In the curve fits, the constants b and c refer to the frequency dependence of the noise ($b\sim-0.5$) and the white noise floor, respectively. As can be seen, the flow did in fact cause increased $1/f$ noise, which can stem from a number of sources, e.g., discontinuities in the flow control, or slipping and turbulence at the outlet, affecting the number of charge carriers in the plasma, as well as the dielectric properties in the gap of the MPS, in turn affecting both the impedance and the distribution of the plasma.

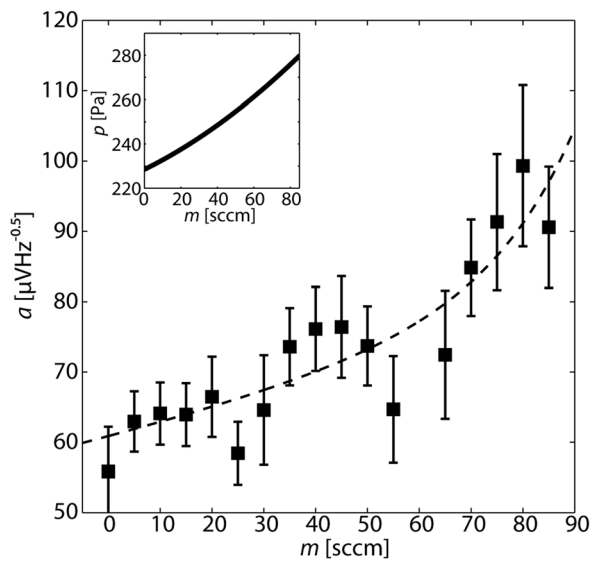

FIG. 14. Flicker noise density as calculated by curve fitting to the noise floor of the recorded spectrum at different CO_2 flow. The inset shows the chamber pressure at different flow rates.

There are several ways of mitigating the $1/f$ noise caused by the flow. For example, the fluidic system could be closed by sealing the gap of the MPS on each side with IR transparent windows, Fig. 15, and using the dual fluidic system as inlet and outlet, respectively. At a sufficiently low pressure, the flow through the gap will turn laminar, and the turbulence, and possibly also the slipping, will vanish. Even better would be measurements under static conditions, i.e., $m=0$, often referred to as batch mode measurements.[16] This would remove both turbulence and discontinuous flow, but new problems relating to pressure control and leakage would arise.

In experiment II, there turned out to exist a maximum S/σ around $P_{in}=36$ dBm, Fig. 13(b). Although S continued to increase for higher P_{in}, σ increased even faster. At $P_{in}=36$ dBm, S started to drop. The instability at low attenuation is explained by heat dissipation from dielectric losses

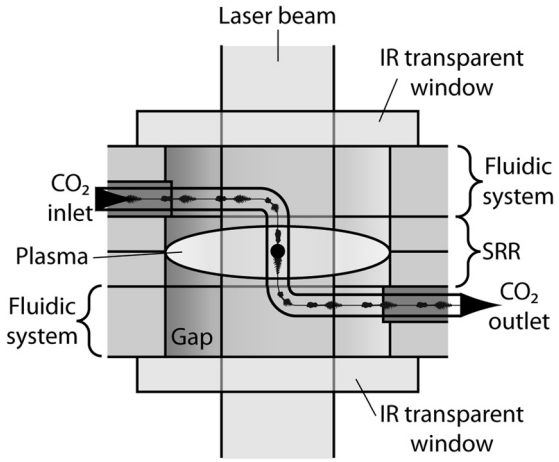

FIG. 15. Schematic view of a closed MPS with integrated fluidic system, possibly reducing turbulence.

and excitation of higher order energy levels in the plasma, causing thermal fluctuations in the system. Excitation of higher order energy levels in the CO_2 could also explain the signal reduction at low attenuation. The S/σ maximum, on the other hand, was explained by the plasma becoming as susceptible as possible to a change in impedance, as seen from the maximum of $\partial U/\partial P_{in}$, without the devices being heated enough to start affecting its stability. Moreover, assuming the first excited vibrational level of the symmetric stretch mode, where the CO_2 molecules are susceptible to absorption of the laser photons, to be Boltzmann populated, there will exist an optimum attenuation where the plasma temperature yields a maximum of CO_2 molecules that can interact with the laser beam without having thermal effects on the device itself. This maximum might be possible to move towards higher P_{in} and consequently higher $\partial U/\partial P_{\text{in}}$ and S/σ by employing active temperature control of the MPS. Finally, the lower signal for high attenuation was explained by the plasma being less susceptible to the OGE due to the lower $\partial U/\partial P_{\text{in}}$.

Experiment III showed less clear S/σ dependence on f_{P}, Fig. 13(c), although the signal dropped as the plasma approached the point where it went out. Like with high attenuation, this was probably due to the plasma being less susceptible to an impedance change close to the critical frequency. There was a slight increase in S/σ at $f_{\text{P}} = 2.75\,\text{GHz}$, i.e., below the resonance frequency of the un-ignited SRR, which might be explained by the resonance frequency being shifted downwards as the plasma was ignited. However, f_{P} did not turn out to be as crucial for S/σ as were m, A_{P}, and f_{C}.

Experiment IV revealed two interesting aspects of the chopper frequency on the measurements. Most important was maybe the background observed for $f_{\text{C}} < 100\,\text{Hz}$, Fig. 13(d). This effect was assumed to be caused by heating of the device by the laser beam. Increasing f_{C} reduced this heating effect by reducing the time for the absorbed energy to be dissipated into the bulk of the device, given the relatively low thermal conductivity of the PCB ($0.71\,\text{Wm}^{-1}\text{K}^{-1}$ as stated by the manufacturer). Even though the time-averaged heat absorption is independent of f_{C}, the periodic heating is longer at lower frequencies, wherefore the periodic heat dissipation is less effective. The plasma was, in contrast to the PCB, subjected to the focused laser radiation and responded much faster to the heating. The response time of the plasma was estimated to around 0.5 ms from Fig. 6. Low-frequency noise might also have contributed to this background. Similarly to the thermal instabilities caused by low attenuation, the thermal background at low f_{C} could be countered by employing active temperature control of the MPS.

The fact that the S/σ ratio had a minimum at $f_{\text{C}} \sim 150\,\text{Hz}$, Fig. 13(d), stemmed both from the above mentioned thermal background, but also from the post-processing of the recorded data. The post-processing only took the first harmonic of S into account, making the measurement sensitive to the waveform of the optogalvanic signal. At low frequencies, the signal had a square shaped waveform. The spectral energy of such a signal is shared by several odd harmonics. Hence, measuring just the first harmonic will give only part of the total signal strength. However, as f_{C} increases, the optogalvanic signal became more and more sinusoidal, resulting in an increasing amount of the spectral energy being represented by the first harmonic, thereby improving both the S/σ ration and the SNR. If lower f_{C} would be of interest, the post-processing should be adapted to cover more harmonics of the signal, thus preserving the SNR even for square shaped signals. However, the oscilloscope used here could only cover 2–3 harmonics, wherefore such optimization is left for future work. The maximum f_{C} could be calculated from the rise and fall time of the OGE, Fig. 6, to around 4 kHz.

Having addressed the limitations and the development opportunities of the system, it is fair to address also its ample advantages. From a sample size point of view, it has been stated that the sample chamber should be filled with CO_2 to an adequate pressure. Although the sample chamber in the experiments reported on here was an external chamber, it was pointed out that the system would benefit from closing the MPS with IR transparent windows, Fig. 15, essentially making the gap equivalent to the sample chamber.

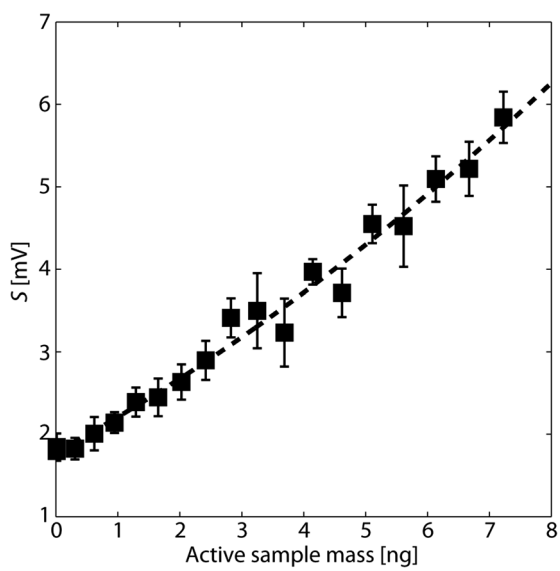

FIG. 16. Optogalvanic signal as a function of the active sample mass, i.e. the mass of carbon in the gap of the MPS.

Furthermore, it is plausible to integrate sample preparation and handling with the MPS by employing microsystems technology, making the total volume of the OGS not much larger than the volume of the gap itself, i.e., tens of microlitre. This should be compared with concurrent OGS systems, which typically has an internal volume of several tens of millilitres. Filling the chamber with CO_2 to the pressure range of experiment I, Fig. 14 (inset), thus only requires nanograms of carbon. This can be seen from the mass of the active carbon, i.e., the mass of the carbon atoms in the gap, at different m in experiment I, which is shown in Fig. 16. The mass was derived from the pressure in the chamber, assuming ideal gas conditions.

VI. CONCLUSION

The applicability of an SRR MPS as the optogalvanic sensor in an OGS was investigated. It was shown that an SRR MPS, equipped with bond-wire plasma probes, could be used for measuring the OGE. The amplitude and stability of the optogalvanic signal were investigated, and the relationships between the signal and different properties of the plasma, and of the OGS system, were analyzed. It was shown that the long-time stability of the system was affected by thermal drift, as well as by direct heating by the laser and by the plasma itself. Moreover, the stability and amplitude of the signal were at a maximum when the plasma was exited with an intensity just below the point where it started to have a thermal effect on the rest of the device. This was explained by the plasma at this point being the most susceptible to the OGE, partly due to Boltzmann population of the first excited vibrational level of the symmetric stretch mode, and partly due to the plasma's sensitivity to small perturbations ($\partial U/\partial P_{in}$). Furthermore, the stability of the signal proved sensitive to the stability of the flow of CO_2 through the MPS, where slipping and turbulence in the flow caused flicker noise in the signal.

A number of methods for stabilizing the signal were discussed. For example, active cooling of the MPS, as well as of the laser and the power electronics, would help reduce both thermal fluctuations and drift, hence improving both the long and short time stability of the signal. Employing a more stable laser, e.g., a single longitudinal mode CO_2 laser, would improve the stability too. Regardless of the stability, such a laser would be necessary for, e.g., isotope ratio OGS, since this requires single-mode, isotope-specific lasing frequencies. Moreover, by incorporating the MPS in a microfluidic system, the flow through the gap could be made laminar, thus mitigating the instability caused by slipping and turbulence. Even more promising, a microfluidic system with valves would enable measurements on static samples, removing instabilities in the flow control in addition to the slipping and turbulence.

An MPS with such a microfluidic system, manufactured by means of microsystems technology, and integrated with systems for sample preparation and handling, would enable OGS with carbon samples as small as nanograms, i.e., almost three orders of magnitude smaller than what is possible with conventional techniques. Initially, measurements of $^{13}C/^{12}C$ ratios would be the most plausible, but even radiocarbon measurements might be possible by employing ICOGS. This would in turn enable completely new kinds of studies, e.g., in the fields of microdosing in medicine, and radiocarbon dating in archaeology.

ACKNOWLEDGMENTS

The Swedish National Space Board is acknowledged for funding the project, and the Knut and Alice Wallenberg foundation is acknowledged for funding the laboratory facilities. Mehran Salehpour and Gerriet Eilers at the Dept. of Physics and Astronomy at Uppsala University are acknowledged for their contribution of both knowledge and hardware.

[1]C. Bronk Ramsey, "Radiocarbon dating: Revolutions in understanding," Archaeometry **50**, 249–275 (2008).
[2]W. F. Libby, "Perspectives: radiocarbon dating," Am. Sci. **44**, 98–112 (1956), available at http://www.jstor.org/stable/27826732.
[3]J. Fabryka-Martin, H. Bentley, D. Elmore, and P. L. Airey, "Natural iodine-129 as an environmental tracer," Geochim. Cosmochim. Acta **49**, 337–347 (1985).
[4]K. Nishiizumi, C. P. Kohl, J. R. Arnold, R. Dorn, I. Klein, D. Fink, R. Middleton, and D. Lal, "Role of in situ cosmogenic nuclides ^{10}Be and ^{26}Al in the study of diverse geomorphic processes," Earth Surf. Process. Landforms **18**, 407–425 (1993).
[5]G. Lappin and R. C. Garner, "Big physics, small doses: The use of AMS and PET in human microdosing of development drugs," Nat. Rev. Drug Discov. **2**, 233–240 (2003).
[6]M. Salehpour, G. Possnert, and H. Bryhni, "Subattomole sensitivity in biological accelerator mass spectrometry," Anal. Chem. **80**, 3515–3521 (2008).
[7]K. L. Spalding, E. Arner, P. O. Westermark, S. Bernard, B. A. Buchholz, O. Bergmann, L. Blomqvist, J. Hoffstedt, E. Naslund, T. Britton, H. Concha, M. Hassan, M. Ryden, J. Frisen, and P. Arner, "Dynamics of fat cell turnover in humans," Nature (London) **453**, 783–787 (2008).
[8]H. Polach, "Evaluation and status of liquid scintillation counting for radiocarbon dating," Radiocarbon **29**, 1–11 (1987), available at https://journals.uair.arizona.edu/index.php/radiocarbon/article/view/1030/1035.
[9]E. Rapkin, "Liquid scintillation counting 1957–1963: A review," Int. J.Appl. Radiat. Isot. **15**, 69–87 (1964).
[10]S.-H. Kim, P. B. Kelly, and A. J. Clifford, "Accelerator mass spectrometry targets of submilligram carbonaceous samples using the high-throughput zn reduction method," Anal. Chem. **81**, 5949–5954 (2009).
[11]M. Ruff, L. Wacker, H. W. Gäggler, M. Suter, H. A. Synal, and S. Szidat, "A gas ion source for radiocarbon measurements at 200 kV," Radiocarbon **49**, 307–314 (2007), available at https://journals.uair.arizona.edu/index.php/radiocarbon/article/view/2930.
[12]T. J. Ognibene, G. Bench, J. S. Vogel, G. F. Peaslee, and S. Murov, "A high-throughput method for the conversion of CO2 obtained from biochemical samples to graphite in septa-sealed vials for quantification of 14C via accelerator mass spectrometry," Anal. Chem. **75**, 2192–2196 (2003).
[13]I. Galli, S. Bartalini, S. Borri, P. Cancio, D. Mazzotti, P. De Natale, and G. Giusfredi, "Molecular gas sensing below parts per trillion: Radiocarbon-dioxide optical detection," Phys. Rev. Lett. **107**, 270802 (2011).
[14]D. E. Murnick, O. Dogru, and E. Ilkmen, "Intracavity optogalvanic spectroscopy. an analytical technique for 14C analysis with subattomole sensitivity," Anal. Chem. **80**, 4820–4824 (2008).
[15]G. Eilers, A. Persson, C. Gustavsson, L. Ryderfors, E. Mukhtar, G. Possnert, and M. Salehpour, "The radiocarbon intracavity optogalvanic spectroscopy setup at Uppsala," Radiocarbon **55**, 3–4 (2013).
[16]E. Ilkmen, "Intracavity optogalvanic spectroscopy—radiocarbon analysis with attomole sensitivity," Ph.D. dissertation (Department of Physics, Rutgers, Newark, NJ, 2009).

[17]D. E. Murnick and B. J. Peer, "Laser-based analysis of carbon isotope ratios," Science **263**, 945–947 (1994).
[18]J. R. de Laeter, J. K. Böhlke, P. De Bièvre, H. Hidaka, H. S. Peiser, K. J. R. Rosman, and P. D. P. Taylor, "Atomic weights of the elements. Review 2000," Pure Appl. Chem. **75**, 683–800 (2003).
[19]A. Persson, G. Eilers, L. Ryderfors, E. Mukhtar, G. Possnert, and M. Salehpour, "Evaluation of intracavity optogalvanic spectroscopy for radiocarbon measurements," Anal. Chem. (published online).
[20]R. D. May and P. H. May, "Solid-state radio frequency oscillator for optogalvanic spectroscopy: Detection of nitric oxide using the 2-0 overtone transition," Rev. Sci. Instr. **57**, 2242–2245 (1986).
[21]F. Iza and J. Hopwood, "Split-ring resonator microplasma: Microwave model, plasma impedance and power efficiency," Plasma Sources Sci. Technol. **14**, 397 (2005).
[22]J. E. M. Goldsmith and J. E. Lawler, "Optogalvanic spectroscopy," Contem. Phys. **22**, 235–248 (1981).
[23]S. Moffatt and A. L. S. Smith, "Temperature perturbation model of the opto-galvanic effect in CO_2 laser discharges," J. Phys. D **17**, 59 (1984).
[24]M. Berglund, G. Thornell, and A. Persson, "Evaluation of a microplasma source based on a stripline split-ring resonator," Plasma Sources Sci. Technol. (submitted).
[25]V. Lekholm, K. Palmer, and G. Thornell, "Schlieren imaging of microthruster exhausts for qualitative and quantitative analysis," Measur. Sci. Technol. **23**, 085403 (2012).
[26]A. Persson, R. Bejhed, H. Nguyen, K. Gunnarsson, B. T. Dalslet, F. W. Østerberg, and M. F. Hansen, "Low–frequency noise in planar Hall effect bridge sensors," Sens. Actuat. A **171**, 212–218 (2011).
[27]X. Zhang and G. Hu, "1/f noise in a two-lane highway traffic model," Phys. Rev. E **52**, 4664–4668 (1995).
[28]F. N. Hooge, "1/f noise is no surface effect," Phys. Lett. A **29**, 139–140 (1969).